

## Quasi-SU(3) Coupling Induced Oblate-Prolate Shape Phase Transition in the Casten Triangle


K. Kaneko,<sup>1,\*</sup> Y. Sun,<sup>2,†</sup> N. Shimizu,<sup>3</sup> and T. Mizusaki<sup>4</sup>

<sup>1</sup>*Department of Physics, Kyushu Sangyo University, Fukuoka 813-8503, Japan*

<sup>2</sup>*School of Physics and Astronomy, Shanghai Jiao Tong University, Shanghai 200240, China*

<sup>3</sup>*Center for Computational Sciences, University of Tsukuba, 1-1-1, Tennodai Tsukuba, Ibaraki 305-8577, Japan*

<sup>4</sup>*Institute of Natural Sciences, Senshu University, Tokyo 101-8425, Japan*

 (Received 1 October 2022; revised 25 November 2022; accepted 12 January 2023; published 3 February 2023)

Shapes and shape evolution in the mass-130 region, including the Te, Xe, and Ba isotopes, have long been a focus of discussion in nuclear physics. This mass region consists of complex many-body systems that can behave in astonishingly simple and regular ways, as classified in the Casten symmetry triangle. By applying the shell model Hamiltonian proposed recently, we carry out calculations using the Hartree-Fock-Bogolyubov plus generator coordinate method, in the large model space containing the  $(1g_{9/2}, 1g_{7/2}, 2d_{5/2}, 2d_{3/2}, 3s_{1/2}, 1h_{11/2}, 2f_{7/2})$  orbits. Based on good reproduction of the experimentally known energy levels, spectroscopic quadrupole moments, and  $E2$  transition probabilities, we identify the quasi-SU(3) couplings across the  $N = 50$  and  $82$  shell gaps, which play a role in driving shape evolution and phase transition discussed in the extended Casten triangle. Specifically, we demonstrate that the quasi-SU(3) coupling mechanism in the proton partner orbits  $(1g_{9/2}, 2d_{5/2})$  tends to drive the system to be more  $\gamma$  soft, and that in the neutron partner orbits  $(1h_{11/2}, 2f_{7/2})$  are responsible for the oblate-to-prolate shape phase transition. With an emphasis on discussing spectroscopic quadrupole moments, our Letter uncovers hidden symmetries from the vast shell-model configurations and adds microscopical insights into the empirical symmetry triangle.

DOI: [10.1103/PhysRevLett.130.052501](https://doi.org/10.1103/PhysRevLett.130.052501)

Shape evolution as a function of the number of protons and neutrons is one of the current topics in nuclear physics. Nuclei with the proton and/or neutron magic number have a spherical shape. Nonspherical shapes begin to develop as nuclei move away from the magic number(s). In the so-called transitional region, which is generally referred to as a developing region where nuclei have no established shape (i.e., neither a sphere nor a well-deformed ellipsoid), rich shape phenomena can emerge. A collection of nuclei with distinct shapes and shape evolution are classified in the Casten symmetry triangle [1], with the three dynamical symmetries U(5), O(6), and SU(3) of the interacting boson model [2] on the vertices. The O(6) limit describes the nuclei of  $\gamma$  softness, corresponding to the picture in the early Willets-Jean model [3]. Adding SU(3) to the original triangle, an extended triangle has been constructed by Jolie *et al.* [4,5], and the O(6) limit is suggested to be a critical point of the phase transition between the prolate and oblate shapes, corresponding to SU(3) and  $\overline{\text{SU}}(3)$ , respectively. All the nuclei in the  $A$ -130 mass region may find a position in the extended triangle. However, questions such as why the SU(3) limit can be split into two and how the two, as the proton and neutron numbers vary, evolve via the O(6) critical point remain open for the microscopic explanation.

Microscopically, nuclear shapes are induced by correlations in systems consisting of neutrons and protons.

The effective nucleon-nucleon ( $NN$ ) interaction gives rise to correlations through configuration mixing of the single-particle orbits occupied by the nucleons. Shapes emerge from the dynamics of many nucleon systems through self-organization [6], exhibiting new collective phenomena that are usually expected from strongly correlated quantum systems [7]. It is important to uncover hidden symmetries from the huge shell-model Hilbert space, which allows for an extraction of the collective dynamics from microscopic effective  $NN$  forces.

To uncover symmetries in the microscopic description of shape evolution, the conventional one-major-shell model is inappropriate. One obvious example is the strongly deformed heavy nuclei such as <sup>154</sup>Sm and <sup>166</sup>Er. To describe those nuclei, a much larger model space is essential [6]. Even for the lighter  $A$ -60 mass region, the extension of model space is necessary to reproduce the rapid change in collectivity from <sup>64</sup>Fe to <sup>66</sup>Fe [8]. The addition of the upper  $2d_{5/2}$  orbit in the  $fpg$  model space is indispensable [9,10].

The joint contribution of  $2d_{5/2}$  to the  $fpg$  model space can be understood by the quasi-SU(3) coupling proposed by Zuker *et al.* [11,12], in which the large  $E2$  collectivity for <sup>64</sup>Cr and <sup>64</sup>Fe near  $N = 40$  [13,14] is explained as the interplay between the quadrupole force and the central field in the subspace with the  $\Delta j = 2$  orbits. In these examples [13,14], the physical backbone is the quadrupole

correlation in the partner orbits ( $1g_{9/2}, 2d_{5/2}$ ) separated by the  $N = 50$  shell gap. The idea of quasi-SU(3) coupling has recently been applied [15] to interpret the sudden enhancement of the  $B(E2; 2_1^+ \rightarrow 0_1^+)$  value within just a few isotopes around  $N = Z = 40$  [16]. Extending the idea, the present authors proposed [17] that by moving one major shell up, one can expect a similar coupling scheme across the  $N = 82$  shell gap of the ( $1h_{11/2}, 2f_{7/2}$ ) type, again satisfying  $\Delta j = 2$ . We have shown [17] that the quasi-SU(3) coupling scheme also plays an important role in the sudden increase of quadrupole collectivity found around  $N = 70$  in the Nd ( $Z = 60$ ) isotopes.

The present Letter discusses the Te, Xe, and Ba isotopes having neutron numbers  $N = 70$ –80, aimed at finding the microscopic origin for shape evolution in the extended Casten triangle. The nuclei to be studied have just a few more protons above  $Z = 50$  and a few less neutrons below  $N = 82$ . Therefore, they are typical transitional nuclei around the O(6) limit in the symmetry triangle. As we shall demonstrate, while both quasi-SU(3) couplings, in the partner orbits ( $1g_{9/2}, 2d_{5/2}$ ) and in the partner orbits ( $1h_{11/2}, 2f_{7/2}$ ), contribute to enhanced E2 collectivity, the former is found to be the main driving force towards  $\gamma$  softness, and the latter is responsible for changing the deformed shapes from oblate to prolate.

To investigate the quasi-SU(3) coupling effect across the  $Z = 50$  and  $N = 82$  shell gaps, one must include the  $1g_{9/2}$  orbit below the  $Z = 50$  and the  $2f_{7/2}$  orbit above the  $N = 82$  shell gap in the major *gdsh*-shell model space. Such a large model space, ( $1g_{9/2}, 1g_{7/2}, 2d_{5/2}, 2d_{3/2}, 3s_{1/2}, 1h_{11/2}, 2f_{7/2}$ ), called *gdshf*, cannot be handled by conventional shell models. For example, the basis dimension for  $^{128}\text{Xe}$  in the  $M$  scheme would reach  $7.6 \times 10^{22}$ , far beyond the current computational capability.

To overcome this difficulty, a promising tool is the Hartree-Fock-Bogolyubov plus generator coordinate method (HFB + GCM) [18] with the code [19]. The method of the angular-momentum-projected GCM with quadrupole-constrained Hartree-Fock basis states was first introduced into shell-model calculations in Refs. [20,21], and its extension has been discussed recently in Ref. [22]. In this type of calculation, the number-projected HFB states are used, in which the pairing correlation is treated explicitly [18,23–25]. We have confirmed that for the current mass region [15,18], the present HFB + GCM approach can provide us with the same quality in results as the exact diagonalization method and the Monte Carlo shell model (MCSM) [26,27].

We adopt the two-body Hamiltonian, called PMMU, which has been proven to work well in a wide range of nuclei [28,29]. It consists of four basic terms:

$$H = H_0 + V_P + V_{QQ} + V_m^{MU}, \quad (1)$$

where  $H_0$  and  $V_P$  are the single-particle Hamiltonian and the (monopole and quadrupole) pairing interaction,

respectively. The  $V_{QQ}$  term in Eq. (1) is the quadrupole-quadrupole interaction, which, in this discussion, is responsible for coupling the particular orbits with  $\Delta j = 2$  to generate the quasi-SU(3) effect. In the present calculation, we employ the same single-particle energies and force strengths as in Ref. [17]. The last term in Eq. (1) is the monopole interaction  $V_m^{MU}$  constructed from the monopole-based universal force [30], which contains a Gaussian central force and a tensor force.

Nuclei of the mass-130 region have long been a focus of discussion in nuclear physics. They have been studied by many models—for example, the Bohr-Hamiltonian approaches derived from the microscopic model [31–34], the shell model [35–37], the SD-pair shell model [38], and the GCM method with the Skyrme-type forces [39]. Some nuclei have been identified as representatives of the symmetry limits in the Casten triangle [40–42]. There are also intensive studies on how shapes evolve from spherical to  $\gamma$  soft or triaxial along isotopic chains [43–47]. Nevertheless, most conclusions are not robust due to the lack of discussion on spectroscopic quadrupole moments ( $Q_s$ ). Recently, Ref. [43] reported experimental data for  $^{130}\text{Xe}$  with energy levels and  $B(E2)$  as well as  $Q_s$  values. They found that several theoretical approaches [35,37,48] and the early phenomenological models [3,49] fail to reproduce the data in Ref. [43]. Very recently, energy levels,  $B(E2)$ , and  $Q_s$  for  $^{126,128}\text{Xe}$  have been observed [50]. We perform the HFB + GCM calculations with the PMMU interaction and find that our shell model can correctly describe the data in Ref. [50].

The most relevant physical observables are the spectroscopic quadrupole moment  $Q_s(I)$  and the electric quadrupole transition probability  $B(E2, I \rightarrow I - 2)$ . Although both are related to matrix elements of the quadrupole operator, they carry different physical information. In particular, the diagonal matrix elements determine  $Q_s(I)$  with a sign, which are measurable quantities [51] and direct indicators for nuclear shapes. In Fig. 1, our calculated  $Q_s$  and  $B(E2; 2_1^+ \rightarrow 0_1^+)$  values (denoted by red lines) are compared with experimental data in the upper and lower graphs, respectively, where the effective charges are taken as  $e_p = 1.0e$  and  $e_n = 0.4e$ . Overall, the calculation reproduces the available experimental data. For comparison, we also present the calculation with the sn100pn interaction [37] in the *gdsh* model space (dashed lines), with the effective charges  $e_p = 1.5e$  and  $e_n = 0.5e$ . The obtained  $Q_s$  values are in reasonable agreement with the data for the Xe and Ba isotopes but not for the Te isotopes. The problem is seen in the calculated  $B(E2)$  values, which largely underestimate the data. Even with adjusted effective charges, it cannot be consistent with both  $Q_s$  and  $B(E2)$ . This comparison suggests the importance of including the  $1g_{9/2}$  and  $2f_{7/2}$  orbits into the *gdsh* shell-model space.

Within the quasi-SU(3) scheme in our *gdshf* calculation, the partner orbits with  $\Delta j = 2$ , ( $1g_{9/2}, 2d_{5/2}$ ) and ( $1h_{11/2}, 2f_{7/2}$ ), are coupled by the  $QQ$  force in Eq. (1).

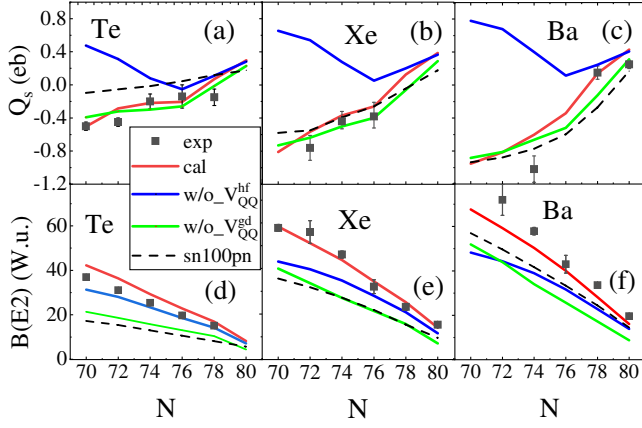


FIG. 1. Spectroscopic quadrupole moment  $Q_s$  and electric quadrupole transition strength  $B(E2; 2_1^+ \rightarrow 0_1^+)$  for Te, Xe, and Ba isotopes in the HFB + GCM calculation using the PMMU model. Experimental data are taken from Refs. [52–56].

First, to see the effect of the quasi-SU(3) coupling between the partner orbits ( $1g_{9/2}, 2d_{5/2}$ ), the  $V_{QQ}^{gd}$  part is removed from the full  $QQ$  interaction [see Eq. (3) in Ref. [15]]. The calculation without  $V_{QQ}^{gd}$  is denoted by green lines in Figs. 1(a)–1(f). It can be seen that for the  $Q_s$  values in Figs. 1(a)–1(c), the results do not differ much from the full calculation. However, in Figs. 1(d)–1(f), the calculated  $B(E2)$  values without  $V_{QQ}^{gd}$  largely underestimate the data. This means that, for all the isotopes, the quasi-SU(3) coupling in the partner orbit ( $1g_{9/2}, 2d_{5/2}$ ) enhances the  $E2$  collectivity. The same conclusion was obtained in Ref. [15].

Next, a striking result occurs when we remove the  $QQ$  interaction between the partner orbits ( $1h_{11/2}, 2f_{7/2}$ ),  $V_{QQ}^{hf}$ . As seen in Figs. 1(a)–1(c), immediately after  $N = 80$ , the calculated  $Q_s$  values without  $V_{QQ}^{hf}$  (blue lines) begin to deviate from that of the full calculation. It is noteworthy that the curves bend at  $N = 76$  to keep the  $Q_s$  value positive (corresponding to an oblate shape). In other words, it is the quasi-SU(3) coupling in the partner orbit ( $1h_{11/2}, 2f_{7/2}$ ) that drives the oblate-to-prolate phase transition. Our result suggests  $N = 76$  as a critical point. Note that this is directly concluded by  $Q_s$  and not from the level energies and  $B(E2)$ s as usual. In Figs. 1(d)–1(f), the  $B(E2)$  values without  $V_{QQ}^{hf}$  underestimate the data, except for the Te isotopes that have  $Z$  numbers close to magicity. No indication of an  $N = 76$  critical point is seen in the  $B(E2)$ s.

In the quasi-SU(3) coupling scheme, the  $QQ$  matrix elements,  $V_{QQ}^{hf}$  and  $V_{QQ}^{gd}$ , correlate with the nucleon occupations. Let us take  $^{128}\text{Xe}$  to demonstrate this. We introduce the variational parameters  $\lambda_1$  and  $\lambda_2$ , which can vary from 0 to 1, and substitute  $\lambda_1 V_{QQ}^{hf}$  and  $\lambda_2 V_{QQ}^{gd}$  for the original terms  $V_{QQ}^{hf}$  and  $V_{QQ}^{gd}$  in the  $V_{QQ}$  interaction. In Fig. 2(a), we see that  $Q_s$  is positive when  $\lambda_1 = 0$ . With increasing  $\lambda_1$ ,  $Q_s$  decreases and becomes  $-0.4$  when  $\lambda_1 = 1$ , which nicely reproduces the experimental data. Stronger  $V_{QQ}^{hf}$  allows neutrons to excite more easily from

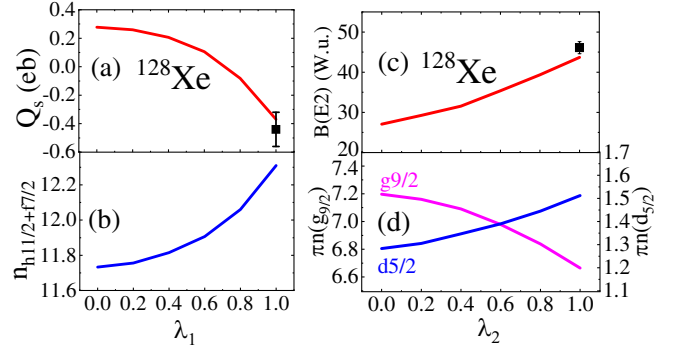


FIG. 2. Variations of  $Q_s$  and  $B(E2; 2_1^+ \rightarrow 0_1^+)$  with the parameters  $\lambda_1$  and  $\lambda_2$  for  $^{128}\text{Xe}$ . See text for explanation.

the  $gds$  shell to the upper-lying  $1h_{11/2}$  and  $2f_{7/2}$  orbits. As seen in Fig. 2(b), the sum of neutron occupations in the  $1h_{11/2}$  and  $2f_{7/2}$  orbits increases correlatively with  $\lambda_1$ . On the other hand, as shown in Fig. 2(c),  $B(E2)$  increases with  $\lambda_2$ , indicating enhanced  $E2$  collectivity. This enhancement is the consequence of proton excitations from  $1g_{9/2}$  to the upper-lying  $2d_{5/2}$  orbit. This can be seen in Fig. 2(d), where, with increasing  $\lambda_2$ , the proton  $1g_{9/2}$  ( $2d_{5/2}$ ) occupancy decreases (increases).

To show that enhanced collectivity induced by the quasi-SU(3) coupling is not only for the ground state but also for low-energy excitations, we present  $B(E2; I \rightarrow I - 2)$  values of excited states for  $^{128}\text{Xe}$  and  $^{130}\text{Xe}$  in Fig. 3. The calculated  $B(E2)$  values correctly reproduce the trend of the data for both  $^{128}\text{Xe}$  and  $^{130}\text{Xe}$ . In the insets of Fig. 3, the theoretical levels excellently reproduce the data for both the ground state and the side bands built on the second excited  $2_2^+$  state. The calculated energy ratios  $E_x(4_1^+)/E_x(2_1^+) = 2.46$  and  $2.37$ , respectively, for  $^{128}\text{Xe}$  and  $^{130}\text{Xe}$ , are in good agreement with the experimental values (2.33 and 2.24). These ratios lie in the middle of the vibration (2.00) and rotation (3.33) limits, and are consistent with  $\gamma$

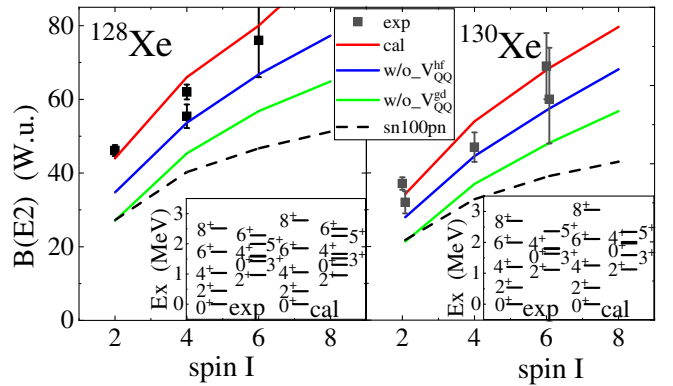


FIG. 3. Comparison of calculated  $B(E2; I^+ \rightarrow I - 2^+)$  with experimental data for (a)  $^{128}\text{Xe}$  and (b)  $^{130}\text{Xe}$ . Insets: comparison of calculated energy levels with data. Experimental data are taken from Refs. [44,55–57].



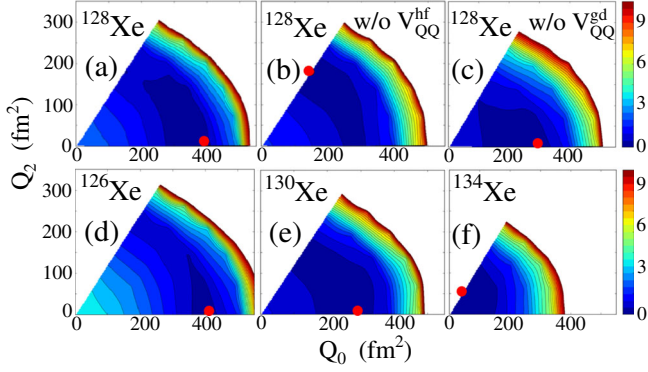


FIG. 4. PES plots for Xe isotopes. (a) PES in the full HFB calculation. (b) PES without  $V_{QQ}^{hf}$ . (c) PES without  $V_{QQ}^{gd}$ . (d)–(f) PES for  $^{126}\text{Xe}$ ,  $^{130}\text{Xe}$ , and  $^{134}\text{Xe}$ , respectively.

softness ( $\sim 2.5$ ). The  $2^+$  side band may be understood as a  $\gamma$  vibrational band. In both isotopes, the first excited  $0_2^+$  state lies above the  $2_2^+$  state, which could be a member of another band. In Fig. 3, we also display the  $B(E2)$  results from the other three calculations, all of which, however, strongly underestimate the data. The calculated  $B(E2)$ s without  $V_{QQ}^{gd}$  are clearly lower than those without  $V_{QQ}^{hf}$ , indicating that  $V_{QQ}^{gd}$  contributes more to enhanced collectivity. On the other hand, the sn100pn calculation with a smaller model space departs considerably from the experimental values for both isotopes.

To directly visualize the quasi-SU(3) coupling effect, the potential energy surface (PES), with collective coordinates  $Q_0$  and  $Q_2$  as variables, is obtained using the quadrupole-constrained HFB method, where  $Q_m = \langle r^2 Y_m^{(2)} \rangle$  with  $m = 0$  or  $2$ . In Fig. 4(a), the PES for  $^{128}\text{Xe}$  is seen to have a prolate energy minimum on the plane spreading in the  $\gamma$  direction. Figures 4(b) and 4(c) show, respectively, the influence of  $V_{QQ}^{hf}$  and  $V_{QQ}^{gd}$ . It is clearly seen in Fig. 4(b) that without  $V_{QQ}^{hf}$ , the energy minimum moves to the oblate side, corresponding to a sign change in  $Q_s$  in Fig. 1(b) for  $N = 74$ . In Fig. 4(c), the PES minimum moves to a smaller  $Q_0$ , meaning that the result without  $V_{QQ}^{gd}$  becomes less deformed. In the lower graphs [(d)–(f)], the shape evolution is shown for a chain of Xe isotopes:  $^{126}\text{Xe}$ ,  $^{130}\text{Xe}$ , and  $^{134}\text{Xe}$ . The PES for  $^{126}\text{Xe}$  ( $N = 72$ ) indicates a prolate minimum on a completely  $\gamma$ -unstable plane, and the shape for  $^{134}\text{Xe}$  ( $N = 80$ ) is nearly spherical.

The above discussions suggest that the quasi-SU(3) coupling scheme across the  $Z = 50$  and  $N = 82$  shell gaps strongly influences the quadrupole collectivity. We have added microscopical insights for the shape evolution discussed in the empirically extended Casten triangle [4]. Without the two key quasi-SU(3) coupling terms,  $V_{QQ}^{gd}$  and  $V_{QQ}^{hf}$ , which act on the  $\Delta j = 2$  orbits and depend sensitively on nucleon occupation, no large quadrupole collectivity could be developed, and no oblate-prolate shape phase transition would occur.

TABLE I.  $B(E2)$  values for positive-parity yrast states and some other collective states in  $^{130}\text{Xe}$  and  $^{130}\text{Ba}$ . Experimental data are taken from Refs. [43,55,56].

$J_i^\pi \rightarrow J_f^\pi$	$^{130}\text{Xe}$ (W.u.)		$^{130}\text{Ba}$ (W.u.)	
	Experimental	Calculated	Experimental	Calculated
$2_1^+ \rightarrow 0_1^+$	32(3)	34	57.9(17)	50.3
$4_1^+ \rightarrow 2_1^+$	47(4)	54	78.9(13)	77.0
$6_1^+ \rightarrow 4_1^+$	$60_{-12}^{+14}$	68	94(6)	92.0
$2_2^+ \rightarrow 2_1^+$	37(3)	48		45.0
$2_2^+ \rightarrow 0_1^+$	0.23(2)	0.20		1.0

Finally, we mention that in the mass-130 region, two or more different shapes can appear in the low-energy region of one nucleus, exhibiting a phenomenon of shape coexistence [58]. Tables I and II use  $^{130}\text{Xe}$  and  $^{130}\text{Ba}$  as examples to discuss their  $B(E2)$  and  $Q_s$  values. For both nuclei, the negative  $Q_s$  for  $2_1^+$  and  $4_1^+$  indicates a prolate shape in the ground-state band. However, for the  $2_2^+$  state in  $^{130}\text{Xe}$ ,  $Q_s = 0.10(10)$  eb corresponds to a less-deformed oblate shape. Furthermore, the magnitude of the measured  $Q_s = -0.38_{-12}^{+14}$  eb for  $2_1^+$  is considerably reduced with respect to the transition quadrupole moment  $|Q_t| = 0.71$  eb estimated from the experimental  $B(E2; 2_1^+ \rightarrow 0_1^+)$  by the simple axial rotor model, which indicates  $\gamma$  instability. In contrast, for  $2_1^+$  in  $^{130}\text{Ba}$ ,  $|Q_t| = 0.96$  eb estimated from  $B(E2; 2_1^+ \rightarrow 0_1^+)$  is close in magnitude to  $Q_s = -1.02(16)$  eb, which is expected for a stable axial-prolate shape. Discussion of shape coexistence involves mixing of configurations belonging to different shapes, which is difficult for a usual empirical classification.

To summarize, the symmetry-based discussion with the Casten triangle can tell us what atomic nuclei do, but it cannot tell us why [1]. Thus, we need a microscopic analysis using methods dealing with nucleons and their interactions. The present Letter has taken a step forward. For the Te, Xe, and Ba isotopes in the mass-130 region, we performed HFB + GCM calculations with the PMMU Hamiltonian. We emphasized that spectroscopic quadrupole moments provide the most decisive information for nuclear shapes. Our detailed analysis for  $^{124-130}\text{Xe}$  demonstrated that the inclusion of the  $1g_{9/2}$  and  $2f_{7/2}$

TABLE II.  $Q_s$  values for positive-parity yrast states and some other collective states in  $^{130}\text{Xe}$  and  $^{130}\text{Ba}$ . Experimental data are taken from Refs. [43,55,56].

$J^\pi$	$^{130}\text{Xe}$ (eb)		$^{130}\text{Ba}$ (eb)	
	Experimental	Calculated	Experimental	Calculated
$2_1^+$	$-0.38_{-14}^{+17}$	-0.26	-1.02(16)	-0.60
$4_1^+$	-0.41(12)	-0.32		-0.77
$2_2^+$	0.1(1)	0.25		0.54

orbits in a major  $gdsh$ -shell model space is essential for describing all the shape characteristics. The  $QQ$  interactions acting on the  $(1h_{11/2}, 2f_{7/2})$  and  $(1g_{9/2}, 2d_{5/2})$  partner orbits are the origin of shape evolution. We have discovered that while the  $QQ$  force acting on the  $(1g_{9/2}, 2d_{5/2})$  orbit pairs tends to drive the evolution toward the  $O(6)$  dynamical limit, that acting on  $(1h_{11/2}, 2f_{7/2})$  robustly changes the shape from oblate to prolate at  $N = 76$ , moving the deformed systems along the  $SU(3)$ - $SU(3)$  side of the extended Casten triangle with  $N = 76$  as a critical point.

Y. S. thanks Yu Zhang for his inspiring discussion and acknowledges support from the National Natural Science Foundation of China (Grants No. 12235003 and No. U1932206). K. K. and N. S. are supported by the Multidisciplinary Cooperative Research Program in CCS, University of Tsukuba (wo22i002). N. S. acknowledges support from the “Program for Promoting Researches on the Supercomputer Fugaku” (No. JPMXP1020200105).

\*kkaneko5319@gmail.com

†Corresponding author.

sunyang@sjtu.edu.cn

- [1] R. F. Casten, *Nat. Phys.* **2**, 811 (2006).
- [2] F. Iachello and A. Arima, *The Interacting Boson Model* (Cambridge University Press, Cambridge, England, 1987).
- [3] L. Wilets and M. Jean, *Phys. Rev.* **102**, 788 (1956).
- [4] J. Jolie, R. F. Casten, P. von Brentano, and V. Werner, *Phys. Rev. Lett.* **87**, 162501 (2001).
- [5] J. Jolie, P. Cejnar, R. F. Casten, S. Heinze, A. Linnemann, and V. Werner, *Phys. Rev. Lett.* **89**, 182502 (2002).
- [6] T. Otsuka, Y. Tsunoda, T. Abe, N. Shimizu, and P. Van Duppen, *Phys. Rev. Lett.* **123**, 222502 (2019).
- [7] P. W. Anderson, *Science* **177**, 393 (1972).
- [8] J. Ljungvall, A. Gorgen, A. Obertelli, W. Korten, E. Clement *et al.*, *Phys. Rev. C* **81**, 061301(R) (2010).
- [9] E. Caurier, F. Nowacki, and A. Poves, *Eur. Phys. J. A* **15**, 145 (2002).
- [10] O. Sorlin *et al.*, *Eur. Phys. J. A* **16**, 55 (2003).
- [11] A. P. Zuker, J. Retamosa, A. Poves, and E. Caurier, *Phys. Rev. C* **52**, R1741 (1995).
- [12] A. P. Zuker, A. Poves, F. Nowacki, and S. M. Lenzi, *Phys. Rev. C* **92**, 024320 (2015).
- [13] A. Gade, R. V. F. Janssens, T. Baugher, D. Bazin, B. A. Brown *et al.*, *Phys. Rev. C* **81**, 051304(R) (2010).
- [14] S. M. Lenzi, F. Nowacki, A. Poves, and K. Sieja, *Phys. Rev. C* **82**, 054301 (2010).
- [15] K. Kaneko, N. Shimizu, T. Mizusaki, and Y. Sun, *Phys. Lett. B* **817**, 136286 (2021).
- [16] R. D. O. Llewellyn, M. A. Bentley, R. Wadsworth, H. Iwasaki, J. Dobaczewski *et al.*, *Phys. Rev. Lett.* **124**, 152501 (2020).
- [17] K. Kaneko, N. Shimizu, T. Mizusaki, and Y. Sun, *Phys. Rev. C* **103**, L021301 (2021).
- [18] N. Shimizu, T. Mizusaki, K. Kaneko, and Y. Tsunoda, *Phys. Rev. C* **103**, 064302 (2021).
- [19] N. Shimizu, HFB + gcm code (unpublished).
- [20] T. Mizusaki, T. Otsuka, Y. Utsuno, M. Honma, and T. Sebe, *Phys. Rev. C* **59**, R1846 (1999).
- [21] K. Hara, Y. Sun, and T. Mizusaki, *Phys. Rev. Lett.* **83**, 1922 (1999).
- [22] D. D. Dao and F. Nowacki, *Phys. Rev. C* **105**, 054314 (2022).
- [23] B. Bally, A. Sanchez-Fernandez, and T. R. Rodriguez, *Phys. Rev. C* **100**, 044308 (2019).
- [24] B. Bally and M. Bender, *Phys. Rev. C* **103**, 024315 (2021).
- [25] B. Bally, A. Sanchez-Fernandez, and T. R. Rodriguez, *Eur. Phys. J. A* **57**, 69 (2021).
- [26] T. Otsuka, M. Honma, T. Mizusaki, N. Shimizu, and Y. Utsuno, *Prog. Part. Nucl. Phys.* **47**, 319 (2001).
- [27] N. Shimizu, T. Abe, Y. Tsunoda, Y. Utsuno, T. Yoshida, T. Mizusaki, M. Honma, and T. Otsuka, *Prog. Theor. Exp. Phys.* **2012**, 01A205 (2012).
- [28] K. Kaneko, T. Mizusaki, Y. Sun, and S. Tazaki, *Phys. Rev. C* **89**, 011302(R) (2014).
- [29] K. Kaneko, T. Mizusaki, Y. Sun, and S. Tazaki, *Phys. Rev. C* **92**, 044331 (2015).
- [30] T. Otsuka, T. Suzuki, M. Honma, Y. Utsuno, N. Tsunoda, K. Tsukiyama, and M. Hjorth-Jensen, *Phys. Rev. Lett.* **104**, 012501 (2010).
- [31] Z. P. Li, T. Niksic, D. Vretenar, and J. Meng, *Phys. Rev. C* **81**, 034316 (2010).
- [32] N. Hinohara, Z. P. Li, T. Nakatsukasa, T. Niksic, and D. Vretenar, *Phys. Rev. C* **85**, 024323 (2012).
- [33] L. Prochniak, *Phys. Scr.* **90**, 114005 (2015).
- [34] A. I. Budaca and R. Budaca, *Phys. Rev. C* **101**, 064318 (2020).
- [35] E. Caurier, F. Nowacki, A. Poves, and K. Sieja, *Phys. Rev. C* **82**, 064304 (2010).
- [36] H. Jin, M. Hasegawa, S. Tazaki, K. Kaneko, and Y. Sun, *Phys. Rev. C* **84**, 044324 (2011).
- [37] B. A. Brown, N. J. Stone, J. R. Stone, I. S. Towner, and M. Hjorth-Jensen, *Phys. Rev. C* **71**, 044317 (2005).
- [38] X. F. Meng, F. R. Wang, Y. A. Luo, F. Pan, and J. P. Draayer, *Phys. Rev. C* **77**, 047304 (2008).
- [39] B. Bally, G. Giacalone, and M. Bender, *Eur. Phys. J. A* **58**, 187 (2022).
- [40] L. Coquard *et al.*, *Phys. Rev. C* **80**, 061304(R) (2009).
- [41] G. Rainovski *et al.*, *Phys. Lett. B* **683**, 11 (2010).
- [42] L. Coquard *et al.*, *Phys. Rev. C* **83**, 044318 (2011).
- [43] L. Morrison, J. Srebrny, T. Berry, A. Boukhari, M. Brunet *et al.*, *Phys. Rev. C* **102**, 054304 (2020).
- [44] L. Coquard *et al.*, *Phys. Rev. C* **82**, 024317 (2010).
- [45] L. Kaya *et al.*, *Phys. Rev. C* **100**, 024323 (2019).
- [46] K. Nomura, N. Shimizu, D. Vretenar, T. Niksic, and T. Otsuka, *Phys. Rev. Lett.* **108**, 132501 (2012).
- [47] C. M. Petrache *et al.*, *Phys. Lett. B* **795**, 241 (2019).
- [48] M. Kortelainen, T. Lesinski, J. More, W. Nazarewicz, J. Sarich, N. Schunck, M. V. Stoitsov, and S. Wild, *Phys. Rev. C* **82**, 024313 (2010).
- [49] A. Davydov and G. Filippov, *Nucl. Phys.* **8**, 237 (1958).
- [50] S. Kisyov, C. Y. Wu, J. Henderson, A. Gade, K. Kaneko *et al.*, *Phys. Rev. C* **106**, 034311 (2022).
- [51] C. Y. Wu *et al.*, *Nucl. Phys.* **A607**, 178 (1996).
- [52] M. J. Bechara, O. Dietzsch, M. Samuel, and U. Smilansky, *Phys. Rev. C* **17**, 628 (1978).
- [53] M. J. Bechara, O. Dietzsch, and J. H. Hirata, *Phys. Rev. C* **29**, 1672 (1984).

- [54] P. J. Rothschild, A. M. Baxter, S. M. Burnett, M. P. Fewell, G. J. Gyapong, and R. H. Spear, *Phys. Rev. C* **34**, 732 (1986).
- [55] Data extracted using the NNDC World Wide Web site from the ENSDF database.
- [56] B. Pritychenko, M. Birch, B. Singh, and M. Horoi, *At. Data Nucl. Data Tables* **107**, 1 (2016).
- [57] G. Jakob *et al.*, *Phys. Rev. C* **65**, 024316 (2002).
- [58] K. Heyde and J. L. Wood, *Rev. Mod. Phys.* **83**, 1467 (2011).